HHS Public Access

Author manuscript

J Glaucoma. Author manuscript; available in PMC 2021 September 01.

Published in final edited form as:

J Glaucoma. 2020 September ; 29(9): 823–830. doi:10.1097/IJG.0000000000001570.

Clinical Utility of Triplicate En Face Image Averaging for Optical Coherence Tomography Angiography in Glaucoma and Glaucoma Suspects

Andrew J. Nelson, BS[1], **Zhongdi Chu, PhD**[2], **Bruce Burkemper, PhD, MPH**[3], **Brenda Ryuna Chang, BS**[1], **Benjamin Xu, MD, PhD**[1], **Ruikang K. Wang, PhD**[2], **Grace M. Richter, MD, MPH**[1]

[1]USC Roski Eye Institute, Department of Ophthalmology, Keck School of Medicine of the University of Southern California, California, United States

[2]Department of Bioengineering, University of Washington, Washington, United States

[3]Departments of Preventive Medicine, Keck School of Medicine of the University of Southern California, California, United States.

Abstract

Purpose: To test the hypothesis that triplicate averaging of the radial peripapillary capillary (RPC) layer improves visualization and diagnostic accuracy of optical coherence tomography angiography (OCTA) for glaucoma.

Methods: This is a cross-sectional study involving 63 primary open angle glaucoma patients and 70 age-matched glaucoma suspects. Triplicate 6x6mm OCTA scans of the optic nerve head were acquired, and the RPC layer was extracted. RPC *en face* images were registered and averaged. Parameters of global entropy (GE), global standard deviation (GSD), local texture correlation (LC), local homogeneity (LH), signal-to-noise ratio (SNR), and intercapillary distance (ICD) were used to measure the change in visualization with averaging. Vessel area density (VAD), vessel skeleton density (VSD), and flux parameters were calculated in a 2.8mm annulus excluding the optic disc. Diagnostic accuracy of these parameters for glaucoma was assessed by calculating area under the receiver operating curve (AUC) values.

Results: 3-frame averaging resulted in decreased GE and GSD (Ps<0.001), and increased LC, LH, SNR, and ICD (Ps<0.001). Averaged images also had reduced VAD, VSD, and flux (Ps<0.001). AUC was significantly increased for VSD after image averaging (p=0.018), while no significant change in AUC was observed for VAD (p=0.229) or flux (p=0.193).

Correspondence and reprint requests to: Grace M. Richter, MD, MPH, Assistant Professor of Ophthalmology, Glaucoma Division, USC Roski Eye Institute, 1450 San Pablo Street, Ste. 4700, Los Angeles, CA 90033, grace.richter@med.usc.edu, Phone: 323-442-6421.

Presentation: Parts of the data in this manuscript were presented at the Association for Research in Vision and Ophthalmology (ARVO) Annual Meeting 2019.

Disclosures: Ruikang K. Wang is a consultant of Carl Zeiss Meditec and holds a patent on the SD-OCTA device from Carl Zeiss Meditec (Dublin, CA). The remaining authors declare no financial disclosure.

Conclusions: Triplicate averaging improves visualization of the RPC layer and the diagnostic accuracy of VSD for glaucoma. The impact of image averaging on OCTA diagnostic performance and other potential applications warrants further exploration.

Précis

Averaging triplicate en face angiograms of the radial peripapillary capillary plexus with optical coherence tomography angiography (OCTA) improves vessel visualization, reduces vessel density parameters, and increases the diagnostic accuracy for glaucoma of one such parameter.

Keywords

Optical coherence tomography angiography; glaucoma; microvasculature; diagnosis; image averaging

INTRODUCTION

Glaucoma is a progressive optic neuropathy characterized by apoptosis of retinal ganglion cells and the subsequent loss of axons in the retinal nerve fiber layer (RNFL).[1] Given the progressive nature of the disease, early diagnosis is essential for effective treatment and optimization of visual outcomes.[2] Currently, glaucoma diagnosis typically involves optic disc examination, gonioscopy, visual field testing, central corneal thickness measurement, intraocular pressure (IOP) measurement, and RNFL thickness measurement via optical coherence tomography (OCT).[3]

Optical coherence tomography angiography (OCTA), which provides *in vivo* assessment of retinal vasculature, may also be a useful tool in glaucoma diagnosis. The high axial resolution of OCTA allows for the selective analysis of discrete microvascular layers of the retina. The radial peripapillary capillary (RPC) layer refers to the microvasculature which supplies the RNFL, and reduced perfusion of the RPC has been implicated in glaucoma pathogenesis.[4-6] Currently, OCTA indices of peripapillary perfusion offer diagnostic accuracy comparable to RNFL thickness as measured by OCT.[7-11] However, given the unique ability of OCTA to quantify vascular defects, OCTA may be able to provide clinical utility for glaucoma diagnosis and monitoring that cannot be offered by OCT alone.[12] For example, OCTA may be more useful than OCT in detecting glaucomatous change when there is concurrent disc gliosis.[13] Furthermore, it has been suggested that combining OCTA and OCT parameters can improve the sensitivity and specificity of glaucoma diagnosis.[12] Consequently, processes which improve the precision and accuracy of OCTA parameters could have an important impact on detecting glaucoma, monitoring its progression, and making treatment decisions.

Factors such as eye motion artifacts, image processing artifacts, and background noise may limit the precision with which OCTA can measure the retinal microvasculature.[14] Multiple B-scan averaging is a technique widely utilized in OCT to reduce noise and improve image quality.[15] Similarly, multiple *en face* image averaging can be used in OCTA. Prior studies have demonstrated that image averaging reduces noise and improves visualization of the choriocapillaris,[16] deep capillary plexus,[17] superficial capillary plexus,[17,18] lamina cribrosa

microvasculature,[19] and RPC,[20] but its impact on the diagnostic utility of OCTA parameters for glaucoma is not known. In this study, we use a custom method of image averaging on triplicate *en face* images of the RPC and hypothesize that averaging improves visualization of the microvasculature, quantitative assessment of its parameters, and the diagnostic accuracy for glaucoma.

MATERIALS AND METHODS

This is a prospective, cross-sectional, observational study approved by the University of Southern California Health Sciences Institutional Review Board. It was conducted in accordance with the Declaration of Helsinki and the Health Insurance Portability and Accountability Act of 1996. All subjects provided informed consent prior to participation.

Participants

All participants were recruited from the glaucoma clinics at the USC Roski Eye Institute over a 13-month period (July 1, 2018 to July 31, 2019). Diagnosis of primary open-angle glaucoma (POAG) was provided by a fellowship-trained glaucoma specialist based on the presence of characteristic optic nerve rim defects on clinical exam, glaucomatous visual field deficits, and an open iridocorneal angle on gonioscopy. Assessment of OCT RNFL thickness data, visual field data (Humphrey 24–2; Zeiss), and intraocular pressure (IOP) measurements were included in the diagnostic clinical examination. Glaucoma suspects (GS) included patients seen in the glaucoma clinic due to suspicion of glaucoma and the need for glaucoma monitoring, but with no clinical evidence of glaucomatous optic neuropathy. Demographic and clinical information including age, sex, history of hypertension and/or diabetes, glaucoma medications, IOP, central corneal thickness, cup-to-disc ratio, and visual field mean deviation was collected from chart review.

OCTA Image Acquisition

All participants underwent 6×6mm triplicate OCTA imaging of the optic nerve head (ONH) region using a spectral domain-OCTA device (Cirrus 5000 HD-OCT with Angioplex, Carl Zeiss Meditec, Dublin, CA). This device has a center wavelength of 840 nm and generates OCTA images using the optical microangiography (OMAG^{c}) algorithm.[21] It also utilizes FastTrac™ motion correction software to reduce artifacts caused by small eye movements during scanning. Each participant received topical proparacaine, tropicamide, and phenylephrine for pupillary dilation prior to imaging. 3 scans centered on the optic nerve head (ONH) were performed in tandem for both eyes of each participant. We acquired 3 frames because Mo et al.[20] demonstrated that the greatest improvement in quantitative metrics in the RPC occurs with averaging of 2 and 3 frames, and acquisition of more images in a clinical setting is impractical. Prior to image processing, image quality was assessed using a standardized quality grading algorithm. Images with missing data, multiple motion artifacts, off-center discs, or signal strength less than 7 were excluded from analysis. Only sets of three good quality images of the same eye from the same visit were analyzed. Prototype semiautomatic segmentation software was used to generate *en face* images of the perfused RPC layer (Cirrus 11.0).

Registration and Averaging

Because small movements between scans are inevitable, images must be registered so that the vasculature is appropriately overlaid. We employed a 3-step registration process using a custom MATLAB program which has been previously reported[16] (MATLAB R2017a; MathWorks, Inc, Natick, MA). The first scan was chosen as the reference for registration. After registration, the images were averaged to generate the single scan image, 2-frame averaged image, and 3-frame averaged image (Figure 1).

Quality Assessment Indices

Image quality assessment indices were calculated for each single frame and 3-frame averaged image using custom MATLAB software. Global entropy[22] (GE), global standard deviation (GSD), local texture correlation[23] (LC), and local homogeneity[24] (LH) are measures of image texture. The binary vessel map was used to segment the flow signal, defined as the intensity within the area of the binary vessel map (I_{signal}), from the noise, defined as the intensity outside the area of the binary vessel map ($I_{background}$), in the *en face* image. The signal-to-noise ratio (SNR) was then calculated as the unitless ratio of the mean signal to the standard deviation of noise.

$$SNR = \frac{\mu_{Isignal}}{\sqrt{\sigma^2_{Ibackground}}}$$

Quantification Indices

The single frame and averaged *en face* images were processed into binary images using customized, interactive quantification software, which has been previously described.[25] This approach uses a combined method of global threshold, hessian filter, and adaptive threshold to extract the binarized image used for quantification. A global threshold of background noise was selected by the user from avascular areas within the ONH. The ONH itself was outlined manually and excluded from quantification, and a 2.8mm annulus around the selected disc margin was selected. Large vessels greater than 32 μm in caliber were subtracted from the image and excluded from quantification. Subsequently, a binary vessel map was generated in which areas of detected vessels are occupied by white pixels and all other areas by black pixels. A skeletonized vessel map was then generated from the binary vessel map. In the skeletonized map, each vessel was represented by a continuous line of single pixels.

Vessel Area Density (VAD) is defined as the unitless ratio of the summation of white pixels in the binary vessel image representing vasculature ($A_{(I,j)}$) to the total number of pixels ($X_{(I,j)}$) comprising the image.

$$VAD = \sum_{i=1,j=1}^{n} A_{(i,j)} \Big/ \sum_{i=1,j=1}^{n} X_{(i,j)}$$

VAD therefore provides information about both vessel caliber and vessel density.

Vessel Skeleton Density (VSD) is defined as the unitless ratio of the sum of white pixels in the skeletonized image ($S_{(I,j)}$) to the total number of pixels ($X_{(I,j)}$) comprising the image.

$$VSD = \sum_{i=1,j=1}^{n} S_{(i,j)} \Big/ \sum_{i=1,j=1}^{n} X_{(i,j)}$$

Because all vessels are one pixel in width in the skeletonized image, VSD reflects relative vessel density but does not take vessel caliber into account.

Intercapillary distance (ICD) was also calculated using the binary vessel map. A reversed binary image was generated within the annulus in which the avascular regions were populated with white pixels. Ellipses that have the same normalized second central moments of area as each pixelated region were generated and their major and minor axes were measured. ICD was defined as the average of the minor axis length for the total number of pixelated regions, representing the shortest distance from one capillary edge to another.

The OMAG^{c} algorithm provides information about blood flow velocity and concentration by comparing OCT signals between consecutive B-scans. Flux is defined as the averaged flow intensity within the detected vasculature in the binary vessel map; it represents the number of blood cells passing through the image cross-section per unit time.

Statistical Analysis

Only GS and patients with POAG, including normal-tension glaucoma, were included in the study. SAS 9.4 software (SAS Institute Inc., Cary, NC) was used for age-matching and data analysis. Candidate GS eyes were age-matched with POAG eyes within a range of 5 years. The matching procedure was performed on all candidate POAG eyes, which included both eyes for some subjects. Of 89 candidate POAG eyes, 87 were paired with an age-matched GS eye. Some of the age-matched GS subjects had scans of both eyes available; for these subjects both eyes were included, resulting in an age-matched dataset with 97 GS eyes and 87 POAG eyes. The dataset was then tested by regressing glaucoma diagnosis on age using generalized estimating equations (GEE), which adjusted for inter-eye correlation, in order to ensure that no statistically significant age difference remained between GS eyes and POAG eyes.

Triplicate images from 97 GS eyes and 87 POAG eyes were analyzed. Wilcoxon signed-rank test was used to non-parametrically test for differences in parameter estimates based on single frame and triplicate averaged images. Similarly, Wilcoxon rank sum test was used to non-parametrically compare the percent reduction in each parameter after image averaging between the POAG group and the GS group. Logistic regression models were used to model glaucoma diagnosis against OCTA parameter values from single frame and averaged images. Predicted probabilities of glaucoma derived from generalized estimating equation (GEE) models were used to calculate sensitivities at fixed levels of specificity. To assess diagnostic accuracy, area under the curve (AUC) was calculated from receiver-operating-characteristics

curve statistics. DeLong's method[26] was used to nonparametrically compare the AUCs of prediction models based on OCTA parameters estimated using single frame images with models based on parameters estimated using triplicate averaged images.

RESULTS

366 subjects participated in the study. Images from 203 participants were excluded due to inadequate image quality, insufficient signal strength, or significant media opacities or vitreous floaters. 30 participants were excluded due to unsuccessful age-matching. 184 eyes from 133 participants were included in the final analysis. Of these, there were 97 GS eyes and 87 POAG eyes (Table 1). GS participants had an average age of 58.6 ± 14.1 years and POAG participants had an average age of 59.6 ± 13.2 years. 38 (54%) GS participants and 29 (46%) POAG participants were female.

Image Quality Indices

Triplicate averaging resulted in reduction in noise and improvement in vessel continuity in the *en face* images (Figure 2). This translated to less granular binary vessel maps and fewer capillary endpoints in the skeletonized vessel maps (Figure 2). We observed significant decreases in global entropy ($p<0.001$) and in global standard deviation ($p<0.001$) for single frames compared to averaged images (Table 2). Significant increases in local signal correlation ($p<0.001$) and local homogeneity ($p<0.001$) were seen for the single frame compared to averaged images (Table 2). There was also a significantly higher SNR in single frame versus averaged images ($p<0.001$) (Table 2). Finally, the mean intercapillary distance was 22.46 μm in single frame images and 25.11 μm in averaged images ($p<0.001$) (Table 2).

Quantitative Parameters

Significant differences in the quantitative indices were observed between single frame and averaged images for both GS and POAG groups (Table 3 and Figure 3). VAD, VSD, and flux values for the single frames were higher compared to the averaged images in both the GS group and the POAG group (ps<0.001). Percent reductions in VAD, VSD, and flux were greater in the POAG group (0.074, 0.076, and 0.102, respectively) than the GS group (0.025, 0.031, and 0.065, respectively, ps<0.001).

Diagnostic Accuracy

AUC values for VAD, VSD, and flux were slightly greater when using the averaged images rather than the single frame (Table 4 and Figure 4). DeLong's method was used to determine whether the differences were statistically significant. A significant increase in AUC was observed for VSD ($p=0.0184$), while trends toward higher AUCs were observed for VAD ($p=0.229$) and flux ($p=0.193$).

DISCUSSION

This study demonstrates that triplicate *en face* image averaging of the RPC significantly improves vessel visualization as measured by image quality metrics, impacts the quantitative assessment of the RPC vasculature, and improves the diagnostic accuracy of one parameter,

VSD, for glaucoma. This is the first study, to our knowledge, to assess the impact of multiple image averaging on the diagnostic utility of OCTA in glaucoma.

Our method of image registration and averaging improved image texture as measured by GE, GSD, LC, and LH, which has been previously demonstrated in the choriocapillaris[16]. We also observed a significant improvement in SNR through triplicate averaging. By averaging multiple frames to a registered reference frame, noise was reduced and the contrast between vessels and background was enhanced, increasing the SNR. Furthermore, we demonstrate that the ICD measurement was significantly higher with averaging. Mo et al. [20] also measured ICD in the RPC with averaging and did not find a significant difference in ICD measurement, even with up to 10 frames averaged. However, they used the average intensity profile within a defined region of interest in the grayscale image to calculate ICD, while our calculation was based upon the minor axis of each pixelated region in the binarized image. Moreover, they measured the distance from the center of one capillary to another, while we measured the distance from the edge of one capillary to another. The difference of these two measurements should be the capillary caliber. Our study also had a larger study population. We hypothesize that as noise is reduced through averaging, the vessel diameter in the binary vessel map becomes sharper and thinner, such that the distance between vessel edges increases. We observe an edge-to-edge ICD of 25.11 μm using the averaged images while histologic studies reveal a center-to-center ICD ranging from 30 to 40 μm.[27] As the typical capillary diameter in the RPC is about 9 μm, the adjusted center-to-center ICD from our calculation would be approximately 34 μm, which is consistent with histologic studies.

Triplicate averaging also influenced the quantitative assessment of the RPC and resulted in decreased VAD, VSD, and flux. These results are similar to the findings of Uji et al.,[28] who demonstrated that multiple image averaging in the superficial and deep retinal layers resulted in lower vessel density (VD) and vessel length density (VLD), which are analogous to our parameters of VAD and VSD, respectively. Notably, Lauermann et al.[18] and Liu et al. [29] also observed lower vessel density in averaged images. Each of the above studies, however, analyzed the impact of averaging on vessel density quantification in the macula, while our study focused on the RPC in the region of the optic nerve head. The lower VAD and VSD is likely explained by a smaller number of total pixels in the binary vessel map and skeletonized vessel map that, due to limitations of noise, meet the threshold for detection as a blood vessel. Flux, however, is the average flow intensity within the area occupied by vessels in the binary vessel map (i.e. average flow intensity / VAD). Because flux is also lower with averaging, averaging must cause a greater reduction in flow intensity detection than in vessel density detection.

Averaging resulted in greater percent reductions in each parameter in the glaucomatous eyes than the GS eyes (Figure 3). We hypothesize that because glaucomatous eyes have, on average, lower vessel density in the RPC, there is also a greater impact of noise interference causing erroneous detection of vasculature in poorly perfused areas. The reduction in noise provided by averaging would therefore enhance the detection of RPC vascular dropout in glaucomatous eyes. The significant improvement in the diagnostic accuracy of VSD for glaucoma lends support to this hypothesis.

Our observation that triplicate averaging results in significant improvement in diagnostic accuracy of VSD, but not VAD or flux, may be explained by differences in the computation and utility of these parameters. Averaging multiple images likely improves image quality through reduction of speckle noises and improved vessel connectivity. Variation in flow signal due to the image capture occurring during different phases of the cardiac cycle likely also could be compensated with averaging. The process of skeletonization is susceptible to noise in binarized vessel maps, therefore a more accurate, better connected and binarized vessel map may lead to more accurate calculation of VSD. With averaging, a skeletonized vessel map is more reflective of the actual RPC plexus, as evidenced by Figure 2F, showing greater vessel continuity and fewer capillary endpoints than the map from a single frame. Furthermore, it is likely that in areas of poorly perfused retina, the smallest vessels are compromised first. Because VSD is not biased by vessel size, it would be the optimal parameter for the detection of capillary dropout. Further studies should assess the impact of averaging a greater number of frames, or a larger sample size, on the diagnostic accuracy of VAD and flux to determine whether the trends we observed towards improvement with averaging become more conclusive.

Despite our finding that image averaging results in higher diagnostic accuracy of VSD for glaucoma, it is not clear whether image averaging improves the clinical utility of OCTA for glaucoma diagnosis. Among each of the three parameters, VAD has the highest diagnostic accuracy when using either single frames or triplicate averaged images, but we did not observe a statistically significant change in the diagnostic accuracy of VAD due to averaging. It may be that we observed the greatest change in the diagnostic accuracy of VSD because VSD is the most susceptible parameter to noise interference, but VAD remains the most optimal parameter for glaucoma diagnosis. Each parameter provides different information, however, such that the impact of averaging on the utility of VSD may still be clinically beneficial. Moreover, it is possible that the linear combination of all of the parameters could have significantly improved diagnostic value when using averaged images compared to the linear combination of all parameters from single images. More detailed analysis is needed, but the findings of this study suggest that image averaging has the potential to significantly impact the diagnostic accuracy of OCTA for glaucoma.

Image averaging may also be useful in longitudinal analyses of glaucomatous eyes in order to detect subtle vascular changes that may indicate progression of disease, but this requires future study. Another potential application of OCTA in glaucoma is the identification of salvageable or “sick” retinal ganglion cells which can recover function with intraocular pressure lowering therapy[30] or other neuroprotective therapies. If salvageable areas of retina are related to perfusion, image averaging could potentially enhance detection of such areas. Moghimi et al.[31] recently reported that OCTA peripapillary vessel density parameters may have a lower measurement floor than RNFL thickness measurements, making OCTA potentially useful for monitoring progression of advanced glaucoma beyond the measurement floor of OCT. The improvement in image resolution provided by averaging may increase the number of detectable steps in advanced glaucoma. Additional research is needed to determine whether image averaging improves the test-retest reliability of OCTA vessel density measurements in order to assess its utility for longitudinal study.

This study has several limitations. The participants in the POAG group had varying histories of treatment interventions, and the impact of surgical procedures and medications on the retinal microcirculation is not well understood. Additionally, there was a slightly greater prevalence of hypertension and diabetes in the POAG group; while this difference was not statistically significant, the extent to which such diseases may have affected RPC perfusion is unknown. Finally, our approach of triplicate averaging requires the acquisition of 3 good quality OCTA images, which can be difficult to achieve in a clinical setting. It should be noted only 133 subjects out of 366 subjects were included in the study, and 203 subjects were excluded due to inadequate image quality. However, it is possible that more rapid and automated acquisition of triplicate images in the future could improve the proportion with high quality scans.

In summary, image averaging is a useful tool for improving visualization of the RPC using OCTA and our results provide evidence that it may improve the diagnostic accuracy of VSD for glaucoma detection. Furthermore, image averaging resulted in greater percent reductions in VAD, VSD, and flux in glaucomatous eyes compared to GS eyes, which suggests that image averaging may also improve detection of vascular dropout in glaucoma. Further research to explore the uses of image averaging in longitudinal assessments of glaucoma patients is needed.

ACKNOWLEDGEMENTS

The authors thank Anoush Shahidzadeh, MPH for her image acquisition support (USC Roski) and Ali Fard, PhD for his image segmentation support (Carl Zeiss Meditec).

Financial Support: This work was supported by the National Institutes of Health (Grants K23EY027855–01, GMR), American Glaucoma Society Young Clinician Scientist Grant (GMR), unrestricted grant to the USC Department of Ophthalmology from Research to Prevent Blindness (New York, NY), and a research device from Carl Zeiss Meditec, Inc. (Dublin, CA). The sponsor or funding organization had no role in the design or conduct of this research.

References

1. Weinreb RN, Leung CKS, Crowston JG, et al. Primary open angle glaucoma. Nat Rev Dis Prim. 2016;2:16067. doi:10.1007/978-1-4614-4172-4_12 [PubMed: 27654570]
2. Heijl A, Cristina Leske M, Bengtsson B, Hyman L, Bengtsson B, Hussein M. Reduction of Intraocular Pressure and Glaucoma Progression Results From the Early Manifest Glaucoma Trial. Vol 120; 2002.
3. Mansberger SL, Stein JD, Herndon LW, et al. Primary Open-Angle Glaucoma Preferred Practice Pattern® Guidelines. Ophthalmology. 2015;123(1):P41–P111. doi:10.1016/j.ophtha.2015.10.053 [PubMed: 26581556]
4. Chen CL, Zhang A, Bojikian KD, et al. Peripapillary retinal nerve fiber layer vascular microcirculation in glaucoma using optical coherence tomography–based microangiography. Investig Ophthalmol Vis Sci. 2016;57:OCT475–OCT485. doi:10.1167/iovs.15-18909 [PubMed: 27442341]
5. Hwang JC, Konduru R, Zhang X, et al. Relationship among visual field, blood flow, and neural structure measurements in glaucoma. Invest Ophthalmol Vis Sci. 2012;53(6):3020–3026. doi:10.1167/iovs.11-8552 [PubMed: 22447865]
6. Yarmohammadi A, Zangwill LM, Diniz-Filho A, et al. Relationship between Optical Coherence Tomography Angiography Vessel Density and Severity of Visual Field Loss in Glaucoma. Ophthalmology. 2016;123(12):2498–2508. doi:10.1016/j.ophtha.2016.08.041 [PubMed: 27726964]

7. Richter GM, Sylvester B, Chu Z, et al. Peripapillary microvasculature in the retinal nerve fiber layer in glaucoma by optical coherence tomography angiography: focal structural and functional correlations and diagnostic performance. Clin Ophthalmol. 2018;12:2285–2296. doi:10.2147/OPTH.S179816 [PubMed: 30510397]
8. Liu L, Jia Y, Takusagawa HL, et al. Optical coherence tomography angiography of the peripapillary retina in glaucoma. JAMA Ophthalmol. 2015;133(9):1045–1052. doi:10.1001/jamaophthalmol.2015.2225 [PubMed: 26203793]
9. Yarmohammadi A, Zangwill LM, Diniz-Filho A, et al. Optical coherence tomography angiography vessel density in healthy, glaucoma suspect, and glaucoma eyes. Investig Ophthalmol Vis Sci. 2016. doi:10.1167/iovs.15-18944
10. Triolo G, Rabiolo A, Shemonski ND, et al. Optical coherence tomography angiography macular and peripapillary vessel perfusion density in healthy subjects, glaucoma suspects, and glaucoma patients. Investig Ophthalmol Vis Sci. 2017;58(13):5713–5722. doi:10.1167/iovs.17-22865 [PubMed: 29114838]
11. Chung JK, Hwang YH, Wi JM, Kim M, Jung JJ. Glaucoma Diagnostic Ability of the Optical Coherence Tomography Angiography Vessel Density Parameters. Curr Eye Res. 2017;42(11):1458–1467. doi:10.1080/02713683.2017.1337157 [PubMed: 28910159]
12. Kwon HJ, Kwon J, Sung KR. Additive Role of Optical Coherence Tomography Angiography Vessel Density Measurements in Glaucoma Diagnoses. Korean J Ophthalmol. 2019;33(4):315. doi:10.3341/kjo.2019.0016 [PubMed: 31389207]
13. Do JL, Sylvester B, Shahidzadeh A, et al. Utility of optical coherence tomography angiography in detecting glaucomatous damage in a uveitic patient with disc congestion: A case report. Am J Ophthalmol Case Reports. 2017;8:78–83. doi:10.1016/j.ajoc.2017.10.009
14. Spaide RF, Fujimoto JG, Waheed NK. Image artifacts in Optical coherence tomography angiography. Retina. 2015;35(11):2163–2180. doi:10.1097/IAE.0000000000000765 [PubMed: 26428607]
15. Sander B, Larsen M, Thrane L, Hougaard JL, Jørgensen TM. Enhanced optical coherence tomography imaging by multiple scan averaging. Br J Ophthalmol. 2005;89:207–212. doi:10.1136/bjo.2004.045989 [PubMed: 15665354]
16. Chu Z, Zhou H, Cheng Y, Zhang Q, Wang RK. Improving visualization and quantitative assessment of choriocapillaris with swept source OCTA through registration and averaging applicable to clinical systems. Sci Rep. 2018;8:16826. doi:10.1038/s41598-018-34826-5 [PubMed: 30429502]
17. Uji A, Balasubramanian S, Lei J, et al. Multiple enface image averaging for enhanced optical coherence tomography angiography imaging. Acta Ophthalmol. 2018;96:e820–e827. doi:10.1111/aos.13740 [PubMed: 29855147]
18. Lauermann JL, Xu Y, Heiduschka P, et al. Impact of integrated multiple image averaging on OCT angiography image quality and quantitative parameters. Graefe's Arch Clin Exp Ophthalmol. 2019;257(12):2623–2629. doi:10.1007/s00417-019-04492-y [PubMed: 31630231]
19. Numa S, Akagi T, Uji A, et al. Visualization of the Lamina Cribrosa Microvasculature in Normal and Glaucomatous Eyes: A Swept-source Optical Coherence Tomography Angiography Study. J Glaucoma. 2018;27:1032–1035. doi:10.1097/IJG.0000000000001069 [PubMed: 30161079]
20. Mo S, Phillips E, Krawitz BD, et al. Visualization of radial peripapillary capillaries using optical coherence tomography angiography: The effect of image averaging. PLoS One. 2017;12(1):e0169385. doi:10.1371/journal.pone.0169385 [PubMed: 28068370]
21. An L, Shen TT, Wang RK. Using ultrahigh sensitive optical microangiography to achieve comprehensive depth resolved microvasculature mapping for human retina. J Biomed Opt. 2011;16(10):106013. doi:10.1117/1.3642638 [PubMed: 22029360]
22. Gonzalez R, Eddins S, Woods R. Digital Image Publishing Using MATLAB. Prentice Hall; 2004.
23. Soh LK, Tsatsoulis C. Texture analysis of sar sea ice imagery using gray level co-occurrence matrices. IEEE Trans Geosci Remote Sens. 1999;37(2):780–795. doi:10.1109/36.752194
24. Cheng H, Li J. Fuzzy homogeneity and scale-space approach to color image segmentation. Pattern Recognit. 2003:1545–1562.

25. Chu Z, Lin J, Gao C, et al. Quantitative assessment of the retinal microvasculature using optical coherence tomography angiography. J Biomed Opt. 2016;21(6):066008. doi:10.1117/1.JBO.21.6.066008

26. DeLong ER, DeLong DM, Clarke-Pearson DL. Comparing the areas under two or more correlated receiver operating characteristic curves: a nonparametric approach. Biometrics. 1988;44(3):837–845. [PubMed: 3203132]

27. Yu PK, Cringle SJ, Yu DY. Correlation between the radial peripapillary capillaries and the retinal nerve fibre layer in the normal human retina. Exp Eye Res. 2014;129:83–92. doi:10.1016/j.exer.2014.10.020 [PubMed: 25447563]

28. Uji A, Balasubramanian S, Lei J, Baghdasaryan E, Al-Sheikh M, Sadda SR. Impact of Multiple En Face Image Averaging on Quantitative Assessment from Optical Coherence Tomography Angiography Images. Ophthalmology. 2017;124:944–952. doi:10.1016/j.ophtha.2017.02.006 [PubMed: 28318637]

29. Liu K, Mehta N, Alibhai AY, Arya M, Sorour O, Ishibazawa A. Effects of enhanced depth imaging and en face averaging on optical coherence tomography angiography image quantification. 2020.

30. Dastiridou A, Chopra V. Potential applications of optical coherence tomography angiography in glaucoma. Curr Opin Ophthalmol. 2018;29(3):226–233. doi:10.1097/ICU.0000000000000475 [PubMed: 29553952]

31. Moghimi S, Bowd C, Zangwill LM, et al. Measurement floors and dynamic ranges of optical coherence tomography and angiography in glaucoma. Ophthalmology. 2019. doi:10.1016/j.ophtha.2019.03.003

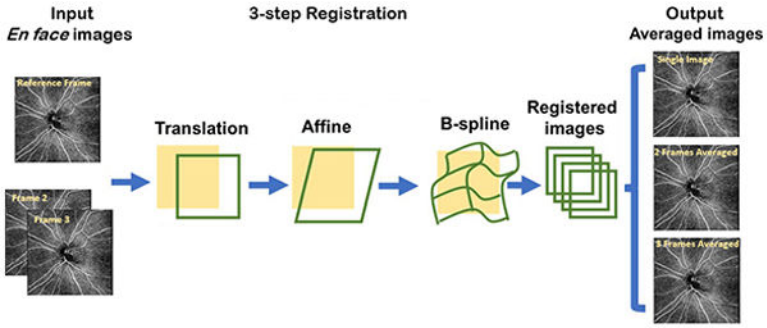

Figure 1.

Illustration of the registration and averaging algorithm used to generate the single registered image, 2-frame averaged image, and 3-frame averaged image.

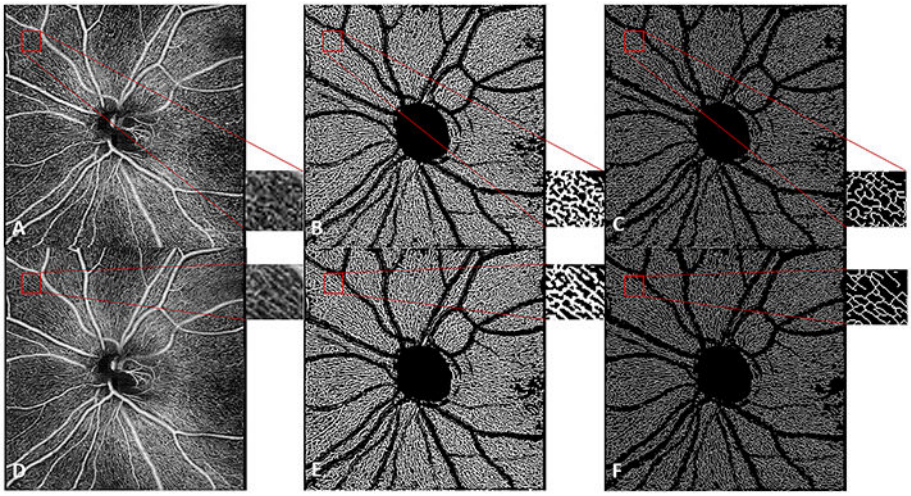

Figure 2.

6x6mm *en face* image of the radial peripapillary capillaries in a glaucoma suspect for the single image (A) and 3-frame averaged image (D) with magnification of selected area. Improved continuity of vessels is seen in the binary vessel maps generated from a single image (B) relative to that from a 3-frame averaged image (E), and in the skeletonized image generated from a single image (C) relative to that from a 3-frame averaged image (F).

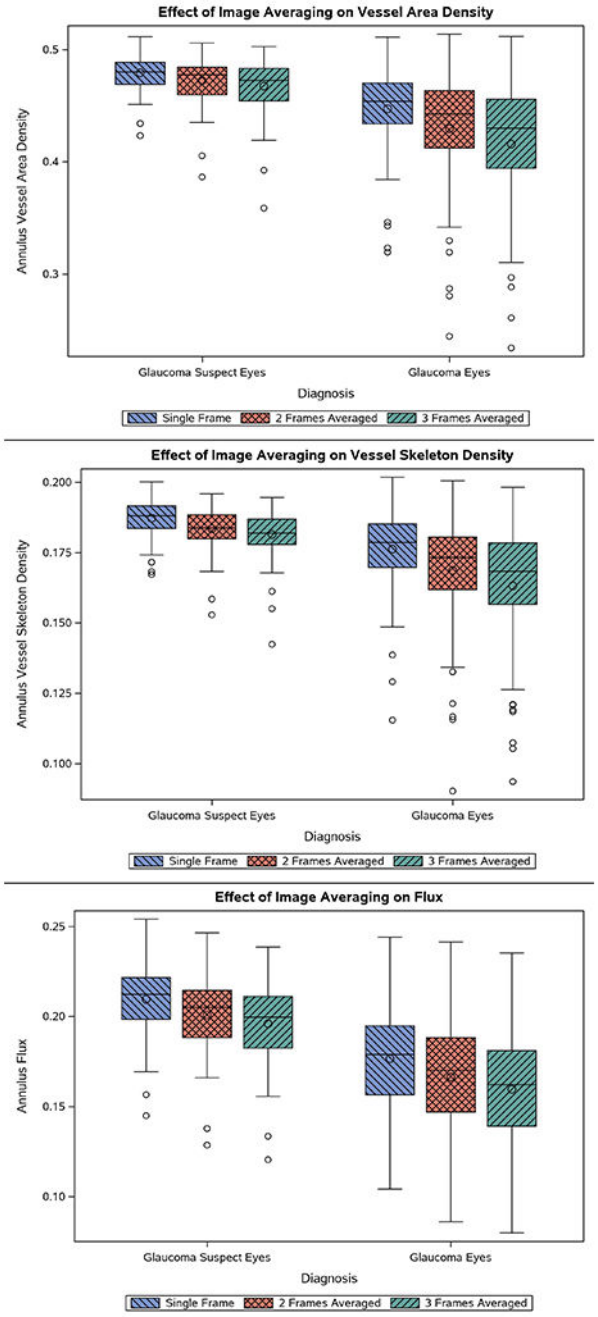

Figure 3.

Differential Effect of Triplicate Image Averaging on Quantitative Indices of Peripapillary Blood Flow in Glaucoma Suspect Eyes and Glaucomatous Eyes. Box plots display the distribution of values for VAD (top), VSD (middle), and flux (bottom). Mean values are successively lower with greater number of frames averaged.

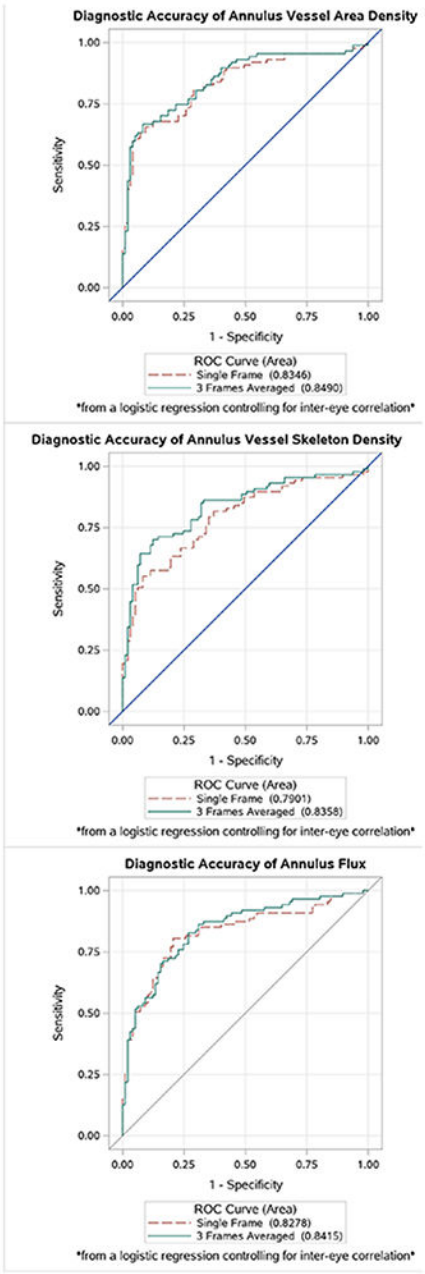

Figure 4.

Area under the receiver operating curve for annulus vessel area density (top), vessel skeleton density (middle), and flux (bottom) in glaucoma using the single image (red dotted line) and the averaged image (green solid line).

Table 1.

Demographic Information for Glaucoma Suspect and Glaucoma Groups

Variables	Glaucoma Suspect Group* (97 eyes from 70 subjects)	Glaucoma Group* (87 eyes from 63 subjects)	P-value†
Age (years)	58.6 (14.1)	59.6 (13.2)	0.661
Female Sex	38 (54.2%)	29 (46.0%)	0.389
Hypertension	15 (21.4%)	18 (32.2%)	0.314
Diabetes	5 (7.14%)	10 (16.9%)	0.105
Glaucoma Medications	0.103 (0.530)	1.430 (1.370)	**<0.001**
Cup-to-disc ratio	0.571 (0.163)	0.784 (0.140)	**<0.001**
Intraocular Pressure (mmHg)	14.70 (3.94)	14.28 (5.23)	0.633
Central Corneal thickness (μm)	549.8 (42.9)	544.2 (44.7)	0.541
Visual field mean deviation (dB)	−0.856 (1.898)	−4.375 (5.617)	**<0.001**

*Continuous variables listed as mean (standard deviation). Categorical variables listed as number (proportion).

†P-values for subject-specific continuous variables were obtained using linear regression from generalized estimating equations (GEE). Significant p-value (<0.05) shown in bold. P-values for subject-specific categorical variables were obtained using chi-squared tests. Significant p-values (<0.05) shown in bold. P-values for eye-specific continuous variables were obtained using t-tests. Significant p-values (<0.05) shown in bold.

Table 2.

Effect of Triplicate Image Averaging on Image Quality Indices

Quality Index	Single Image*	3-Frame Averaging*	P-value†
Global Entropy	0.9743 (0.9704, 0.9782)	0.9483 (0.9438, 0.9529)	**<0.001**
Global Standard Deviation	0.2040 (0.2021, 0.1927)	0.1907 (0.1887, 0.2058)	**<0.001**
Local Correlation	0.6691 (0.6670, 0.6712)	0.6932 (0.6913, 0.6951)	**<0.001**
Local Homogeneity	0.8602 (0.8588, 0.8615)	0.8750 (0.8737, 0.8764)	**<0.001**
Signal-to-Noise Ratio	2.0656 (2.0284, 2.0845)	2.1876 (2.1594, 2.2158)	**<0.001**
Intercapillary Distance (μm)	22.4569 (22.0762, 22.8376)	25.1112 (24.5177, 25.7057)	**<0.001**

*All values listed as mean (95% confidence interval).

†P-values obtained from Wilcoxon signed-rank test. Significant p-value <0.05 shown in bold.

Table 3.

Effect of Triplicate Image Averaging on Quantitative Indices of Peripapillary Blood Flow

	Glaucoma Suspect Eyes				Glaucoma Eyes			
Index	**Single Image***	**2 Frames Averaged***	**3 Frames Averaged***	**p-value†**	**Single Image***	**2 Frames Averaged***	**3 Frames Averaged***	**P-value†**
Vessel Area Density	0.479 (0.476, 0.482)	0.472 (0.468, 0.476)	0.467 (0.463, 0.472)	**<0.001**	0.447 (0.440, 0.455)	0.429 (0.419, 0.440)	0.416 (0.404, 0.427)	**<0.001**
Vessel Skeleton Density	0.187 (0.186, 0.189)	0.183 (0.182, 0.185)	0.181 (0.180, 0.183)	**<0.001**	0.176 (0.173, 0.179)	0.169 (0.165, 0.173)	0.163 (0.159, 0.168)	**<0.001**
Flux	0.210 (0.206, 0.213)	0.201 (0.197, 0.205)	0.196 (0.192, 0.200)	**<0.001**	0.177 (0.170, 0.183)	0.166 (0.160, 0.173)	0.160 (0.153, 0.166)	**<0.001**

*Values listed as mean (95% confidence interval).

†P-values obtained from Wilcoxon signed-rank test comparing single frame value to 3-frame averaged image value

Table 4.

Area Under the Receiver Operating Curve (AUC) for Annulus Blood Flow Indices in Glaucoma and Glaucoma Suspects

Index	Single Frame AUC*	Triplicate Averaging AUC*	P-value†
Vessel Area Density	0.8346 (0.7744, 0.8938)	0.8490 (0.7914, 0.9067)	0.229
Vessel Skeleton Density	0.7901 (0.7239, 0.8564)	0.8358 (0.7757, 0.8959)	**0.018**
Flux	0.8278 (0.7657, 0.8899)	0.8415 (0.7837, 0.8992)	0.193

*Values listed as AUC (95% confidence interval).

†P-values obtained from DeLong's method. Significant p-value <0.05 shown in bold.